*Journal of Structural Geology*, Vol. 11, No. 1/2, pp. 51 to 64, 1989
Printed in Great Britain

0191-8141/89 $03.00 + 0.00
Pergamon Press plc

# The origin of *S–C* mylonites and a new fault-zone model*

TOSHIHIKO SHIMAMOTO†

Institute of Geology and Mineralogy, Faculty of Science, Hiroshima University, Hiroshima 730, Japan

(*Received* 2 *February* 1988; *accepted* 10 *October* 1988)

**Abstract**—This paper presents a synthesis of experimental data on mechanical behaviour and deformation textures of simulated halite shear zones with special regard to the internal structures of *S–C* mylonites and their mechanical implications. Halite is the only mineral so far for which a complete transition between brittle shearing deformation to fully ductile shearing flow in the dislocation glide regime has been studied experimentally under large shear strains that may be encountered along faults or plate boundaries. Moreover, deformation textures in the shear zones are similar to those of mylonites and cataclasites. Thus the experimental results provide an insight into the petrogenesis of fault rocks, mylonites in particular, and the establishment of a realistic fault model.

Between the brittle regime and the fully ductile regime (i.e. pressure-insensitive inelastic regime), there exists a wide and distinct regime called 'semiductile' in which deformation textures are nearly identical to those developed in the ductile regime, yet the shear resistance is pressure-dependent, and potentially unstable fault motion can occur in the low pressure part. In cooking salt shear-zone experiments, the characteristic texture in the semiductile and ductile regimes is foliation resembling mylonitic foliation, which formed in the direction of maximum elongation. In the semiductile regime, nearly homogeneous shearing deformation, characterized by the formation of uniform and pervasive foliation, changes into heterogeneous deformation after a critical shear strain and this strain localization induces potentially unstable fault motion. The primary mode of internal slip after the strain localization is slip along *Y* Riedel shears, parallel to the shear-zone boundary, interconnected with $R_1$ and some *P* Riedel shears. These shear surfaces of concentrated deformation are very similar to the internal structures of so-called '*S–C* mylonites'. Hence, the semiductile regime is the primary candidate for the formation of *S–C* mylonites, and at least some *S–C* mylonites must have formed at seismogenic depths. This interpretation is consistent with recently reported interlaced pseudotachylytes and mylonites. It is also shown that the size of recrystallized halite grains (presumably mostly postdeformational) decreases with increasing shear strains, but not with the shear stress, and this is consistent with the grain-size reduction with strain concentration which has been confirmed for many mylonites in the world. Thus, estimation of flow stress from recrystallized grains needs to be done with great care and might often be erroneous.

Existing fault models are critically examined from the viewpoint of the halite experiments, and a new fault model is proposed whereby fault zones are divided into brittle, semibrittle, semiductile and ductile regimes with increasing depth. The shear resistance of faults is highest in the semiductile regime, and the seismogenic depth is likely to extend down to the upper part of this regime. The semiductile regime thus emerges as an area of primary interest with regard to the petrogenesis of many *S–C* mylonites, modelling of large and great shallow earthquakes along pre-existing faults and plate boundaries, and quantitative evaluation of the mechanical interactions of plates across their boundaries.

## INTRODUCTION

UNDERSTANDING the deformation mechanisms along large-scale faults and plate boundaries is of fundamental significance in solving many tectonic problems such as modelling large shallow earthquakes and quantitative evaluation of the mechanical interaction of neighbouring plates. A simple, but widely used fault-zone model is that of Sibson (1977, 1983) which subdivides a fault zone into frictional and quasiplastic regimes (A to B and B to C, respectively, in Fig. 1). In the frictional regime where temperature is low, cataclasis predominates over plastic deformation to form incohesive and cohesive cataclasites, and fault motion is seismogenic. The upper limit of the shear resistance in this regime is given by the empirical equation of Byerlee (1978) for the frictional strength of many brittle rocks. In the quasiplastic regime, on the other hand, temperature is high, the major constituent minerals deform plastically to form mylonites, and the fault motion is accommodated by aseismic shearing deformation of fault-zone rocks. The shear resistance of faults in this regime is given by the high-temperature flow law of rocks and it falls off rapidly with increasing depth because of the softening effect of temperature. To the first approximation, this quasiplastic regime corresponds to the lower crustal weak zone in the continental lithosphere or to the asthenosphere in the mantle (Bird 1978, Brace & Kohlstedt 1980, Kirby 1980, 1985, Chen & Molnar 1983).

Although simple and attractive, Sibson's model needs to be re-examined closely for the following reasons. Firstly, the onset of intracrystalline gliding, the most important mechanism of plastic deformation, varies with slip system and from mineral to mineral, and hence the shift in the deformation mechanism from cataclasis to gliding is inevitably gradual. The semibrittle and semiductile deformations (e.g. Carter & Kirby 1978, Shimamoto & Logan 1986) are not fully incorporated in the model, perhaps mainly due to the lack of relevant experimental data. As will be argued later, the semibrittle and semiductile regimes are likely to be much wider than indicated in Fig. 1. Secondly, large and great thrust-type earthquakes along subducting plate boundaries initiate mostly from the depths of 30–50 km,

* To the memory of late Professor Kazuaki Nakamura.

† Address from 1 February 1989: Earthquake Research Institute, University of Tokyo, Tokyo 113, Japan.

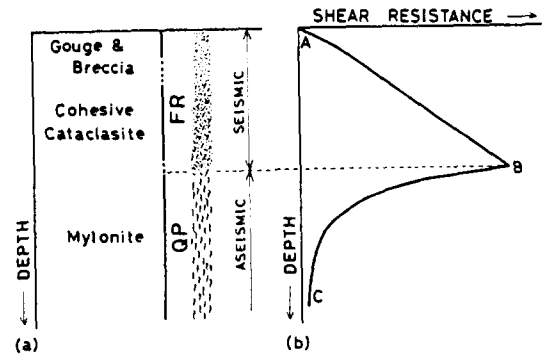


Fig. 1. Schematic diagrams illustrating the fault-zone model of Sibson (1977, 1982, 1983). (a) and (b) show the frictional (FR) and quasi-plastic (QP) regimes together with their corresponding dominant fault rocks and the depth profile of fault strength, respectively. The seismogenic depth corresponds to the frictional regime. The representation of the strength profile in the manner shown in (b) was proposed by Bird (1978) and Goetze & Evans (1979) (see Brace & Kohlstedt 1980, and Kirby 1980 for more discussions).

immediately below the estimated depth for the formation of high-pressure-type metamorphic rocks which commonly display evidence of intense ductile and plastic deformation (Shimamoto 1985). Thus, contrary to the model in Fig. 1, these earthquakes do appear to initiate at depths where deformation is predominantly plastic. Thirdly, intermingled association of pseudotachylytes with mylonites has been found recently at several places in the world (Sibson 1980, Grocott 1981, Passchier 1982, 1984, Hobbs *et al.* 1986), and it was inferred from this association that the seismogenic depth extends well into the pressure-insensitive ductile regime, i.e. the quasiplastic regime in Fig. 1 (Sibson 1980, Hobbs *et al.* 1986, fig. 17). However, the lower portion of a subducting plate boundary rebounds aseismically over a period of several decades following a great thrust-type earthquake (Shimazaki 1974, Thatcher & Rundle 1979) and therefore the seismogenic depth does not extend well into the asthenosphere (Shimamoto 1985). This strongly suggests that the depth range at least for repeatable earthquakes along faults or plate boundaries actually does not extend into the fully ductile regime. The fault-zone model thus remains very controversial at this time.

A geological approach aimed at understanding the deformation mechanisms along faults at various depths is to analyze the deformation structures and textures of rocks along exhumed faults. Sibson's (1977) work is a pioneering attempt along this line. Perhaps the most exciting finding in fault-related fabrics in the last decade is the recognition of a class of rocks called '*S–C* mylonites'. In fact, most of the following leading papers on the internal structures of *S–C* mylonites have appeared in this *Journal* during its first 10 years (Berthé *et al.* 1979, Knipe & White 1979, Jégouzo 1980, Platt & Vissers 1980, Ponce de Leon & Choukroune 1980, White *et al.* 1980, Simpson & Schmid 1983, Lister & Snoke 1984, Platt 1984, O'Brien *et al.* 1987, among many others). The descriptions in these and other papers have revealed that a common feature of *S–C* mylonites is the development of internal shear surfaces cutting the mylonite foliation. Although the occurrence of such mylonites is almost universal, the origin of the shear surfaces and their mechanical implications have only been speculated on up to the present time.

This paper is intended to show how the results from a recent series of experiments on simulated halite shear zones at room temperature (Shimamoto 1985, 1986a, Shimamoto & Logan 1986, Hiraga & Shimamoto 1987, Knapp *et al.* 1987) can be used to establish a realistic fault model and to explore the origin of *S–C* mylonites. Deformation along faults should range from brittle deformation near the surface to fully ductile flow at depths. The halite experiments have allowed the first documentation of a complete spectrum of large-strain behaviour from brittle deformation to the ductile flow in the low-temperature dislocation-glide regime (i.e. from A to around B in Fig. 1) (cf. Kirby 1980). Moreover, these experiments produced textures remarkably similar to those of mylonites, including well-developed foliation, patterns of shear surfaces in *S–C* mylonites, and increasing grain-size reduction with strain concentration (e.g. Tullis *et al.* 1982). Thus, the experimental results are very relevant to the problems addressed above.

The main experimental results and their current interpretations are summarized in the first two sections. Then the last two sections compare the textures developed in halite shear zones with those of *S–C* mylonites and propose a revised fault model based mainly on experimental data. Although halite can only be used as an analog of geologically important silicates, there are no fundamental differences in deformation mechanisms between this and other minerals (see Carter & Hansen 1983, Handin *et al.* 1986). I believe that the halite experiments serve as a useful guide not only for further close examination of mylonites (*S–C* mylonites in particular) and cataclasites along exhumed faults but also for conducting similar but more difficult experiments on silicates with improved techniques. The fault model proposed herein is reported in abstracts by Shimamoto (1986b, 1988).

## *Terminology*

Much confusion exists in the literature as to the usage of widely-used terms, 'ductile' and 'plastic' (see Rutter 1986). These are used in this paper as mechanical and microstructural terms, respectively. That is, 'ductile' is used to refer to inelastic deformation for which the flow stress or shear resistance is nearly independent of the normal stress acting on the shear zone or on faults (see Kirby 1980). The term, 'fully ductile', is used when this pressure independence is emphasized. 'Plastic' is used to refer to inelastic deformation by microscopic mechanisms such as intracrystalline gliding, recrystallization, diffusive mass transfer and solution transfer, contrary to the term 'cataclastic'. The strain localization within halite shear zones was recognized in brittle and intermediate regimes, but strain rarely became localized in fully ductile regimes. Descriptive terms such as 'uniform' and 'localized' are used to describe the nature of deformation, rather than using genetic terms. The ductile regime in the above sense is described also as 'plastic

regime' or as 'quasiplastic regime' in about half of the relevant literature, and these original terms are retained in this paper where the relevant papers are quoted.

## BEHAVIOUR OF SIMULATED HALITE SHEAR ZONES

### *Experimental procedures*

Using a standard triaxial apparatus described by Handin *et al.* (1972), about 60 experiments were conducted on 0.3–1.0 mm thick, compacted halite shear zones along the precut surfaces of cylindrical specimens of Tennessee sandstone (see the inset diagram of Fig. 2). Experiments were carried out at room temperature, at room humidity, at confining pressures of up to 250 MPa (kept constant during the tests) and with a slip rate along the precut surface ranging from 300 down to 0.003 $\mu$m $s^{-1}$ ($\simeq$ 10 cm $yr^{-1}$), following the procedures described in Shimamoto & Logan (1981). Measured stress and displacement were corrected for apparatus distortion, change in contact area and the jacket strength (see Shimamoto 1977, Shimamoto *et al.* 1980). Displacement rate along the precut surface was either kept constant or changed in a step-wise manner (e.g. Fig. 2).

Reagent-grade NaCl (about 0.1 mm in grain size) and cooking salt (natural halite of unknown origin, 0.2–0.3 mm in grain size) were used as the halite layers after appropriate precompaction of halite grains. The thickness of the shear zone was estimated from its weight assuming zero porosity. No permanent deformation of the Tennessee sandstone, even adjacent to the precut surface, was recognized in these tests, and the deformation of the halite shear zones was close to simple shear. The average finite shear strain reached during many of these tests amounted to 40–70, almost one order of magnitude greater than that attained in other similar experiments (Friedman & Higgs 1981, Knapp *et al.* 1987). It will be argued later that the attainment of such large shear strains was the most important key to the success of the present series of experiments.

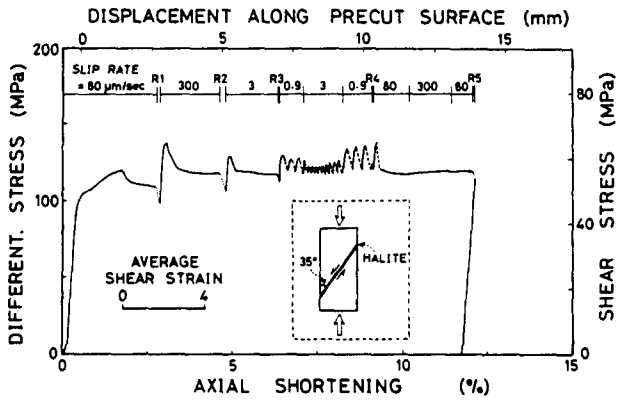


Fig. 2. A typical stress–shortening curve for a specimen of Tennessee sandstone with 0.3 mm thick layer of compacted cooking salt, deformed at room temperature and at a confining pressure of 70 MPa (run number H06 in Shimamoto & Logan 1986, table 1). The slip rate along the precut surface, given near the top of the diagram, was changed either abruptly or after a pause of several minutes in the loading. Dashed lines indicate abrupt slip events during stick–slip, and the dotted lines beneath R1–R5 denote stress relaxation just after the loading motor was turned off. The specimen assembly is shown in the inset diagram.

### *Summary of mechanical data*

Experimental results on the steady-state or nearly steady-state shear resistance of synthetic halite shear zones under large shear strain are compiled in Figs. 3 and 4 in order to display the general features of the transition from brittle to ductile behaviours. Most of these data were collected from velocity-stepping experiments (e.g. Fig. 2), in which the slip rate along the precut surface was changed either abruptly or with a pause of several minutes in the shortening after the shear resistance approached a nearly steady-state, or after regular stick–slip was attained. Cooking salt shear zones exhibit essentially the same trends, although their behaviour is somewhat more variable and is notably more unstable (see Shimamoto 1986a, Shimamoto & Logan 1986, Hiraga & Shimamoto 1987). The essence of the mechanical behaviour may be summarized as follows.

(1) The shear stress sustainable by the synthetic halite shear zones, shown in Fig. 3, is slightly smaller than that for many brittle rocks that were compiled by Byerlee (1978) at confining pressures below about 50 MPa, but it

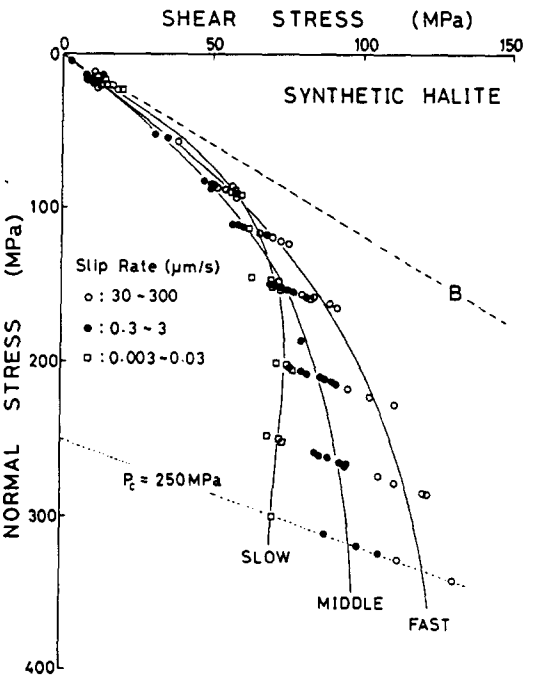


Fig 3. Shear stress vs normal stress on the simulated halite shear zones at steady-state or nearly steady-state sliding (compiled from Shimamoto 1986a, Hiraga & Shimamoto 1987). The shear zones consist of 0.3–0.5 mm thick, dry layers of compacted synthetic halite. Data are arranged in three groups for different ranges of slip rates. When stick–slip occurs, a regular stick–slip portion is selected and the stresses at the initiation of abrupt slip are plotted. The confining pressure is given by the intercept of the abscissa with a line drawn parallel to the fine broken line through each datum point. The dashed line (B) indicates the frictional strength for many brittle rocks (Byerlee 1978).

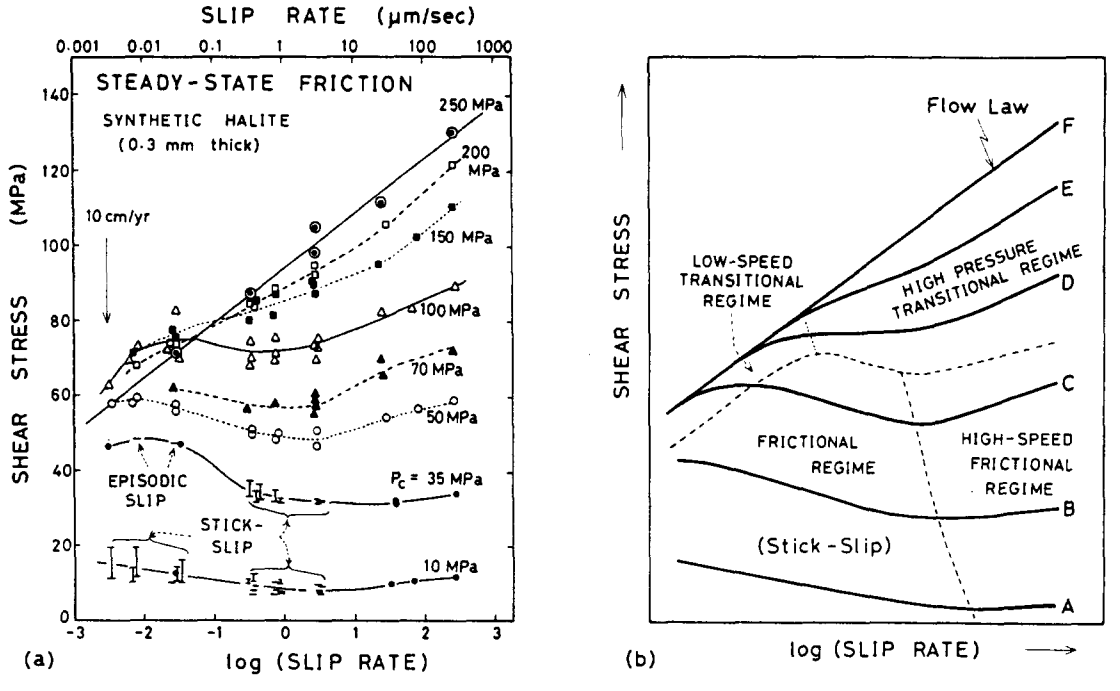


Fig. 4. (a) Steady-state or nearly steady-state shear resistance of a 0.3 mm thick, dry layer of synthetic halite plotted against the common logarithm of slip rate based on eight tests conducted at confining pressures as specified on the curves (Shimamoto 1986a). (b) A schematic diagram illustrating the velocity dependence of the shear resistance (see text for the explanation). The shear resistance during stick–slip is shown by the shear stresses at the onset and at the stop of abrupt slip events, tied with a vertical bar. The run at a confining pressure of 35 MPa is the second run that was performed on the specimen deformed at 70 MPa, and it exhibits somewhat different trends from other runs conducted on initially undeformed specimens.

deviates markedly from his relationship at higher confining pressures and becomes nearly insensitive to the normal stress at confining pressures above about 100 MPa at slow slip rates, above 200–250 MPa at intermediate slip rates, and above about 250 MPa at fast slip rates. Thus in the case of halite, Byerlee's empirical relationship for the frictional strength of brittle rocks does not extend in a straight manner into the fully ductile regime (cf. Figs. 1 and 3).

(2) The halite shear zone seems to be fully ductile and in the plastic regime, at a confining pressure of 250 MPa, since its shear resistance is nearly independent of normal stress at all slip rates (Fig. 3). The shear resistance, $\tau$, increases linearly with an increase in the logarithm of the slip rate, $\dot{\delta}$, at that pressure (Fig. 4a). The deformation within the shear zone is close to homogeneous simple shear at this pressure (see next section), and hence the linear relationship between $\tau$ and the logarithm of $\dot{\delta}$ can be expressed as:

$$\dot{\gamma} = A \exp(a\tau), \tag{1}$$

where $\dot{\gamma}$ is the shear strain rate, $A = 1.38 \times 10^{-10}\,s^{-1}$ and $a = 0.177\ MPa^{-1}$ (Shimamoto 1986a, in press). An equally good fit to the same data is obtained assuming a power law of the form:

$$\dot{\gamma} = q\,\tau^n \tag{2}$$

with $q = 5.56 \times 10^{-37}\ MPa^{-n}\ s^{-1}$ and $n = 17.3$ (Shimamoto 1986a, fig. 4). That the exponential flow law or the power law with large $n$ value holds for the shearing deformation of halite at a confining pressure of 250 MPa indicates that halite is in the dislocation-glide regime at room temperature and at that pressure (see Poirier 1985).

(3) At low confining pressures, the friction–velocity relationship is very similar to that for brittle rocks (Dieterich 1978, Blanpied *et al.* 1987); that is, friction decreases linearly with an increase in the logarithm of $\dot{\delta}$ at slow slip rates (frictional regime), and it increases slightly with increasing $\dot{\delta}$ at fast slip rates (high-speed frictional regime) (see Fig. 4). At very slow rates, where the frictional resistance exceeds the flow stress at that slip rate, the negative velocity dependence in the frictional regime changes into a positive dependence and the shear resistance is given by the flow laws above (see Shimamoto 1986a, fig. 5).

(4) As the confining pressure increases, the frictional regime shrinks, the high-speed frictional regime expands, and the friction–velocity relationship changes gradually into the flow law (Fig. 4). Thus the change in the behaviour from brittle to ductile regimes is completely gradational.

(5) Stick–slip occurs only in the frictional regime with the negative velocity dependence, consistent with the theoretical prediction of Rice & Ruina (1983). Cooking salt shear zones exhibit stick–slip at confining pressures to 70 MPa (e.g. Fig. 2), whereas stick–slip for synthetic halite was recognized at pressures only up to 35 MPa. Hence the slip behaviour of cooking salt is notably more unstable than synthetic halite, presumably because of impurities in the former.

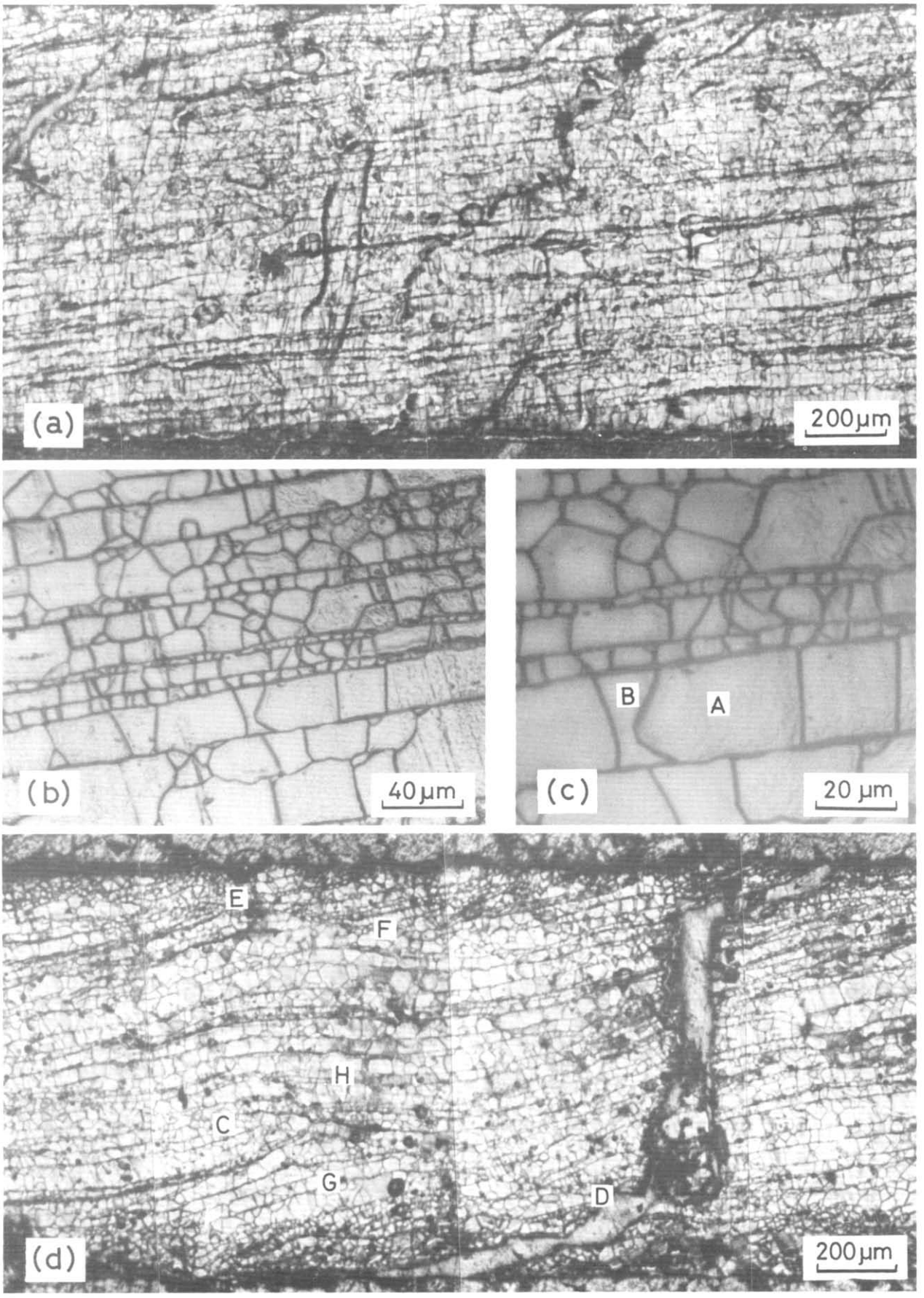


Fig. 5. Photomicrographs under reflected light showing various deformation textures in halite (cooking salt) shear zones deformed at room temperature. The sense of shear is all right lateral. (a) Uniformly and well-developed foliation across the shear zone (confining pressure during the test, $P_c$ = 150 MPa; the average shear strain at the location of photomicrograph, $\gamma$ = 13). (b) Close-up of well-developed foliation defined by straight and parallel grain boundaries ($P_c$ = 70 MPa, $\gamma$ = 30). (c) Further close-up of the central part of (b). (d) Incipient heterogeneous deformation characterized by the wavy-shaped foliation ($P_c$ = 100 MPa, $\gamma$ = 14.2). Foliation is discontinuous across CD and EF, along which the foliation seems to be dragged right-laterally. *(Continued)*

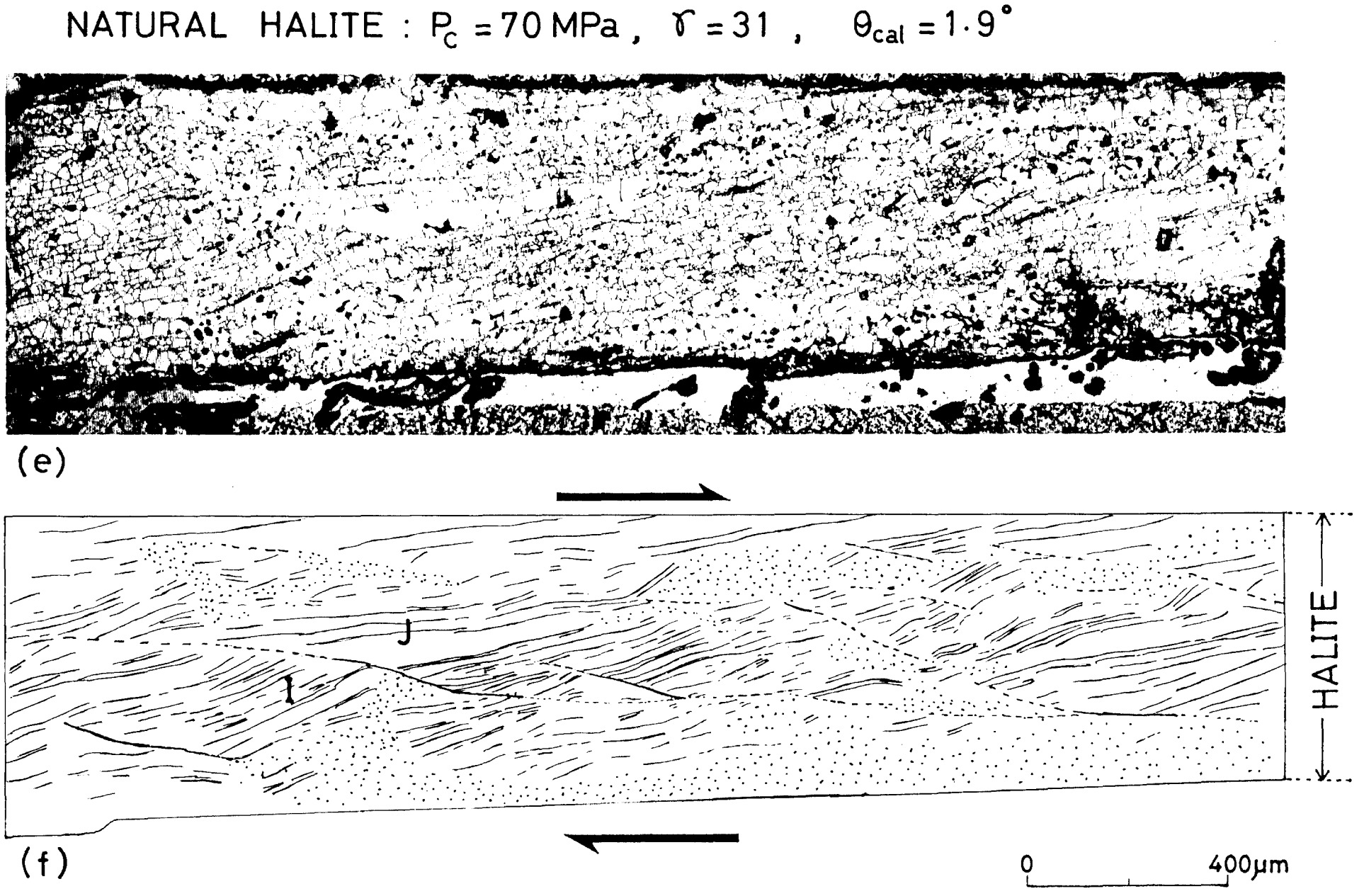


Fig. 5 *continued*. (e) Heterogeneous deformation showing distorted foliation ($P_c$ = 70 MPa, $\gamma$ = 31). (f) Sketch of (e) showing foliation in solid lines, fairly sharp discontinuities in heavy solid lines, and structureless portions in dots. (a)–(d) are taken from Shimamoto & Logan (1986), and (e) and (f) are unpublished data of Hiraga & Shimamoto.

## TEXTURES OF SHEARED HALITE

Microscopic deformation processes within halite shear zones are summarized in this section and are compared with the structures of *S–C* mylonites in the next section. Microscopic observations were made on polished specimens under reflected light with a polarizing microscope, after etching grain boundaries with a small amount of saliva (Shimamoto & Logan 1986, Hiraga & Shimamoto 1987). Deformation textures developed at confining pressures below about 30 MPa are essentially the same as those developed in brittle fault gouges (see Hiraga & Shimamoto 1987) and are not relevant to later discussions. Hence, emphasis will be placed upon the textures developed at higher pressures.

### *Foliation and its origin*

Highly deformed halite is very unstable and is easily susceptible to recrystallization, so that the halite in deformed shear zones had been recrystallized almost completely at the time of observation. The only texture that convincingly reflects the deformation processes in the semiductile and ductile regimes is well-developed foliation in cooking salt shear zones which has the following characteristics and origin.

(1) The foliation is defined by straight and continuous alignment of grain boundaries (Figs. 5a–c). Textures suggestive of grain-boundary migration are preserved at various places; e.g. the grain boundary between grains A and B in Fig. 5(c) seems to have migrated leftward. The zone bounded by straight grain boundaries often consists of typical recrystallized grains with well-developed triple junctions (Fig. 5c) (see also Knapp *et al.* 1987). This type of foliation is peculiar to cooking salt shear zones, and it differs from the foliation defined by elongated calcite grains (Friedman & Higgs 1981), and from the ghost structures defined by elongated visible impurities developed in shear zones consisting of crushed natural halite (Knapp *et al.* 1987). However, when the foliation is developed uniformly and pervasively throughout the shear zones (e.g. Fig. 5a), the orientations of these three types of foliation all agree closely with the orientation of maximum elongation that is estimated from the measured displacement and the shear zone thickness, assuming homogeneous simple shear (Fig. 6). The angle between the foliation and the shear-zone boundary decreases monotonically during progressive simple shear, so that the concept of steady-state foliation after Means (1981) is not applicable to these types of foliation.

(2) The origin of the remarkably straight and continuous grain boundaries (Figs. 5a & b), although not perfectly clear, appears to be related to the effects of impurities such as various nutriments on the surface of cooking salt grains (Shimamoto & Logan 1976). Plastically deformed halite grains must have been extremely flattened in these large-strain experiments to make the original grain surface straight and planar on the flattened sides (e.g. the axial ratio of the strain ellipse is about 170

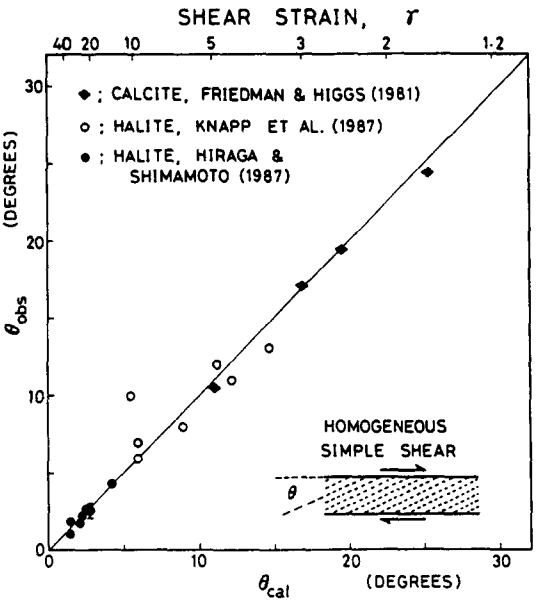


Fig. 6. The measured orientation ($\theta_{obs}$) of homogeneously developed foliation within simulated halite and calcite shear zones plotted against the predicted orientation ($\theta_{cal}$) of the maximum elongation assuming homogeneous simple shear (compiled after Friedman & Higgs 1981, Hiraga & Shimamoto 1987, Knapp *et al.* 1987). The diagonal line indicates the one to one correspondence between $\theta_{obs}$ and $\theta_{cal}$. The vertical bar on the lower-left corner indicates typical standard deviation of measurements in Hiraga & Shimamoto (1987). The shear zones tested by Hiraga & Shimamoto (1987) and by Knapp *et al.* (1987) consist, respectively, of cooking salt and of crushed natural halite.

in the shear zone shown in Fig. 5a). The movement of the flattened grain surface was presumably hindered by the presence of impurities, even during the dynamic or static recrystallization to form the foliation. If this is correct, the straight grain boundary coincides with the flattened grain surface and the foliation should coincide with the orientation of maximum elongation (data shown by solid circles in Fig. 6).

(3) The development of foliation has been recognized at all confining pressures above 30 MPa (Hiraga & Shimamoto 1987, fig 8), so that plastic deformation of halite does occur at comparatively low pressures where the shear resistance, $\tau$, depends markedly on the normal stress, $\sigma_n$, on the shear zone (Fig. 3). Quite importantly, the foliation developed at low pressures is nearly identical in microscopic features to that formed in the pressure-insensitive ductile regime at a confining pressure of 250 MPa. Such an apparently ductile but pressure-dependent deformation was called 'semiductile' (Shimamoto & Logan 1986) in order to distinguish it from semibrittle deformation characterized by the obvious coexistence of plastic and cataclastic deformation (Carter & Kirby 1978).

(4) A puzzling problem is the origin of the observed pressure dependence of the shear resistance in the semiductile regime. Note that the foliation in this regime also forms in the direction of maximum elongation; e.g. the abundant data by Knapp *et al.* (1987), shown by open circles in Fig. 6, were taken from halite shear zones deformed at a confining pressure of 70 MPa, well within the semiductile regime. This indicates that almost all of

the shear strain was accommodated by ductile and homogeneous plastic strain. On the other hand, the observed pressure dependence does suggest that some kind of frictional process is involved in the shearing deformation of halite in the semiductile regime, although there is no textural evidence indicative of this when foliation is uniform and pervasive. Shimamoto (in press) suggests that the pressure dependence shows up because the von Mises criterion of ductility is not met in the semiductile regime; that is, the number of independent slip systems is less than 5. One possibility is that {110} ⟨1$\bar{1}$0⟩ is the only slip system operative for which only two of six {110} systems are independent (Grove & Kelly 1963, Nicolas & Poirier 1976), although this is as yet unconfirmed, owing to the complete recrystallization within the shear zones. Whatever the origin of the pressure dependence, it is remarkable that almost negligible, presumably cataclastic deformation induces a marked pressure dependence of the shear resistance. The significance of this with respect to the petrogenesis of mylonites will be discussed in later sections.

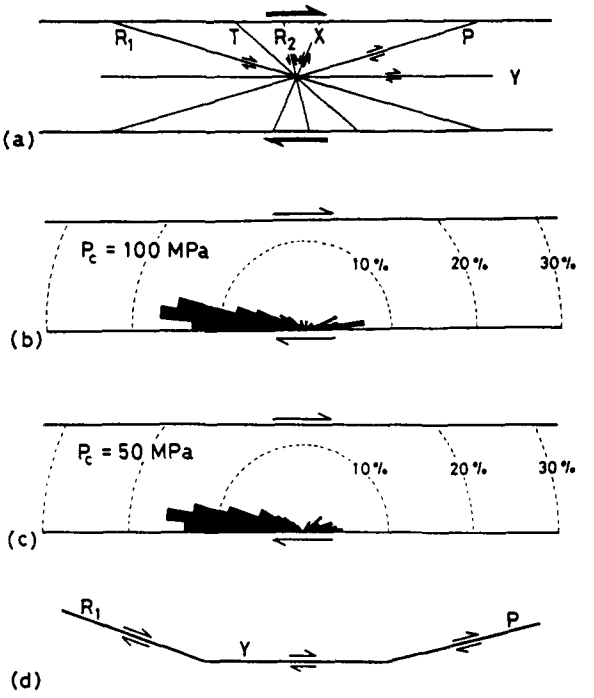


Fig. 7. Orientation of relatively straight discontinuities cutting foliation within halite (cooking salt) shear zones (simplified from Hiraga & Shimamoto 1987). (a) A complete set of Riedel shears and their notations (Bartlett *et al.* 1981). (b) and (c) Rose diagrams, shown by the frequency in per cent, indicating the orientation of the discontinuities within a shear zone deformed at a confining pressure as specified in each diagram. The numbers of measurements in (b) and (c) are 230 and 130 for one and three specimens, respectively. (d) Typical mode of internal slip along *Y* Riedel shears that are interconnected by the displacement along $R_1$ and *P* Riedel shears.

*Strain localization after a critical shear strain*

When the shear strain reaches a certain critical value which depends on the confining pressure (see a later section), the homogeneous shearing deformation described above changes into heterogeneous deformation with the following general features (Shimamoto & Logan 1986, Hiraga & Shimamoto 1987).

(1) Figure 5(d) displays an example of incipient heterogeneous deformation with wavy-shaped foliation which is discontinuous across CD and EF. These discontinuities lie at about 15° to the shear-zone boundary and have the same orientation as $R_1$ Riedel shears (Fig. 7a). The foliation is slightly dragged along them showing the correct sense of $R_1$ shear. In the neighbourhoods of points G and H in Fig. 5(d), the foliation is rotated counterclockwise and clockwise, respectively, relative to the general trend of foliation in the right-hand side of the photomicrograph. These senses of rotation are opposite to that of the movement along $R_1$ shear between C and D, and the rotation of foliation seems to be the external rotation associated with the displacement along $R_1$ shear (Platt & Vissers 1980, fig. 4). Such external rotation is a common mode of bending of foliation even when deformation becomes even more heterogeneous (e.g. I and J in Fig. 5f). Foliation is often folded at large shear strains as described by Hiraga & Shimamoto (1987).

(2) Frequency histograms showing the orientations of the discontinuities of foliation (Figs. 7b & c) indicate that they are mostly $R_1$ and *Y* shears, with some *P* shears (cf. Figs. 5e & f). The orientation of $R_1$ very roughly coincides with the predicted orientation from the angle of internal friction, $\phi$; e.g. $\phi$ = 23–27° at a confining pressure of 50 MPa (Fig. 3), and the angle, $\theta$, between $R_1$ and the shear-zone boundary has a broad maximum at 5–15° ($\theta = \phi/2$ if the orientation of the maximum compression in the shear zone is assumed to be 45° to the boundary). However, the shear surfaces have been rotated and distorted considerably during large shearing deformation. Development of such Riedel shears strongly suggests that uniform plastic deformation becomes localized when the plastic strain reaches a certain threshold value and that some sort of brittle deformation overlaps the plastic deformation, although no direct textural evidence of cataclastic deformation has survived due to the complete recrystallization of the halite grains. A typical mode of internal slip is displacement along $R_1$, *Y* and some *P* Riedel shears that are interconnected with each other (Fig. 7d).

*Size of recrystallized grains*

The size of the recrystallized grains is not related to the steady-state or nearly steady-state shear stress (Shimamoto & Logan 1986, fig 9, Knapp *et al.* 1987, fig 15). Knapp *et al.* (1987, fig. 14) have also shown that the sizes of porphyroblasts and large neoblasts in the halite shear zones deformed at a confining pressure of 70 MPa first increase with increasing shear strain, exhibit a maximum at a shear strain of about 5, then decrease monotonically and approach a constant value at a shear strain of 12–14. This strain dependence of the size of recrystallized grains has been substantiated by grain-size measurement in the trailing edge of a cooking salt shear

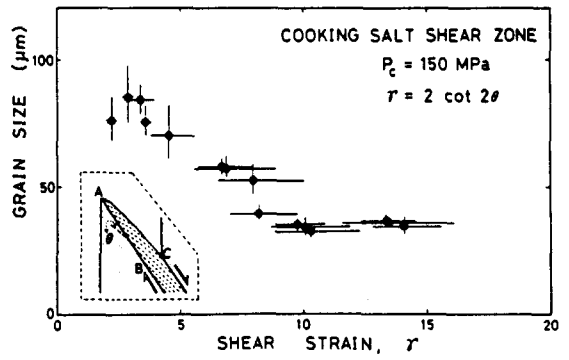


Fig. 8. Size of recrystallized grains plotted against the shear strain in the trailing edge of a cooking salt shear zone deformed at a confining pressure of 150 MPa. The shear strain, $\gamma$, was estimated from the angle, $\theta$, between the foliation and the shear-zone boundary, using the formula in the upper right-hand corner of the diagram which is based on the assumption of homogeneous simple shear (e.g. Nicolas & Poirier 1976). Grain sizes were measured by use of an intercept method (Smith & Guttman 1953, Christie & Ord 1980). The horizontal and vertical bars indicate one standard deviation of the measured grain sizes and shear strains.

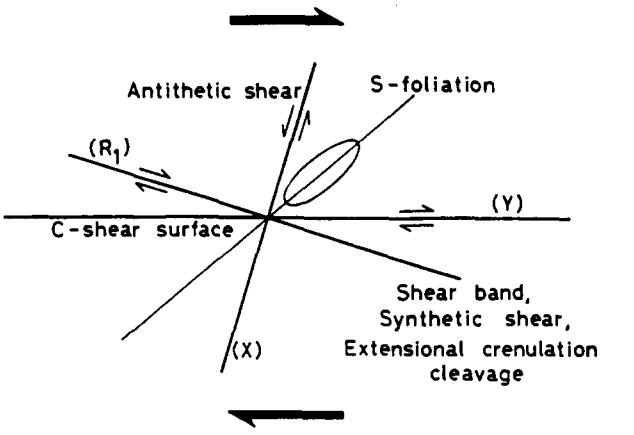


Fig. 9. Schematic diagram illustrating planar fabric of *S–C* mylonites and corresponding Riedel shears shown in parenthesis.

zone, where the shear strain increases progressively from A to BC in the inset diagram of Fig. 8. The results in Fig. 8 are very consistent with those of Knapp *et al.* (1987), although there are small differences in the overall values of grain size, in the shear strain at which the maximum grain size occurs, and in the shear strain at which the grain size becomes nearly constant.

## COMPARISONS WITH *S–C* MYLONITES

### *Structures of* S–C *mylonites and their origin*

The microstructures of so-called *S–C* mylonites from many parts of the world have been described in the past decade (Berthé *et al.* 1979, Knipe & White 1979, Jégouzo 1980, Platt & Vissers 1980, Ponce de Leon & Choukroune 1980, White *et al.* 1980, Simpson & Schmid 1983, Lister & Snoke 1984, Platt 1984, Brunel 1986, Vauchez 1987). Although the structures are variable in fine details, they share a common feature of planar fabric as illustrated in Fig. 9. The mylonite foliation or *S*-foliation is disrupted by three types of shear surfaces: (1) *C*-shear surfaces parallel to the shear-zone boundary (*C* stands for cisaillement or shear; Berthé *et al.* 1979 among many others); (2) synthetic shears developed at a small angle to the shear-zone boundary, also called shear bands (e.g. Simpson & Schmid 1983), extensional crenulation cleavage (Platt & Vissers 1980) or *C'*-shears (Vauchez 1987); and (3) much less common but distinct antithetic shears (Simpson & Schmid 1983, Vauchez 1987). The term '*C*-surface' is used broadly for all of these discrete surfaces, in some of the literature (e.g. Lister & Snoke 1984), but it will be used in a narrow sense in this paper to refer only to the shear surface parallel to the shear zone.

It is clear at a glance that these discrete surfaces in *S–C* mylonites have similar orientations and senses of movement to *Y*, $R_1$ and *X* Riedel shears (cf. Figs. 7 and 9), and presumably they formed by similar mechanisms. The only notable difference is that the *P* surface in cooking salt shear zones have not been identified in the mylonites. It seems possible that *P* surfaces may form nearly parallel to the *S*-foliation in the mylonites and may have been overlooked. In any case *P*, *X* and $R_2$ Riedel shears in cooking salt shear zones are not abundant, so the discrepancy is perhaps not very significant. Another difference is that unlike the discrete shear zones in mylonites, the discontinuous zones cutting the foliation in cooking salt shear zones now consist of an aggregate of recrystallized grains (Shimamoto & Logan 1986, fig. 14). This difference probably arises from the difference in the degree of recrystallization, and is not fundamental.

The order of formation of *S* and other shear surfaces in natural *S–C* mylonites has not yet been resolved, although some authors (e.g. Lister & Snoke 1984) suggest that *S*-surfaces developed prior to the formation of the shear surfaces. In the halite experiments, the order of the formation of these surfaces is clear, as described in the previous section: that is (1) uniform and pervasive foliation in the orientation of maximum elongation, then (2) $R_1$ Riedel shears after a critical shear strain is reached, and finally (3) other Riedel shears upon further deformation.

### *Mechanical implications*

Despite almost universal occurrence of the shear surfaces in *S–C* mylonites, their mechanical significance is largely unexplored. The halite experiments have, however, revealed that the strain localization associated with the formation of Riedel shears has distinct mechanical significance, as outlined below.

The change in mechanical behaviour from the brittle to ductile regime can be seen best at the intermediate displacement rate across the shear zone (Fig. 4). The mechanical behaviour was classified into flow and friction types as schematically shown in Fig. 10(a). The flow-type behaviour is intrinsically stable and is characterized by a gradual and monotonic change in the shear stress toward the steady-state value upon a step change

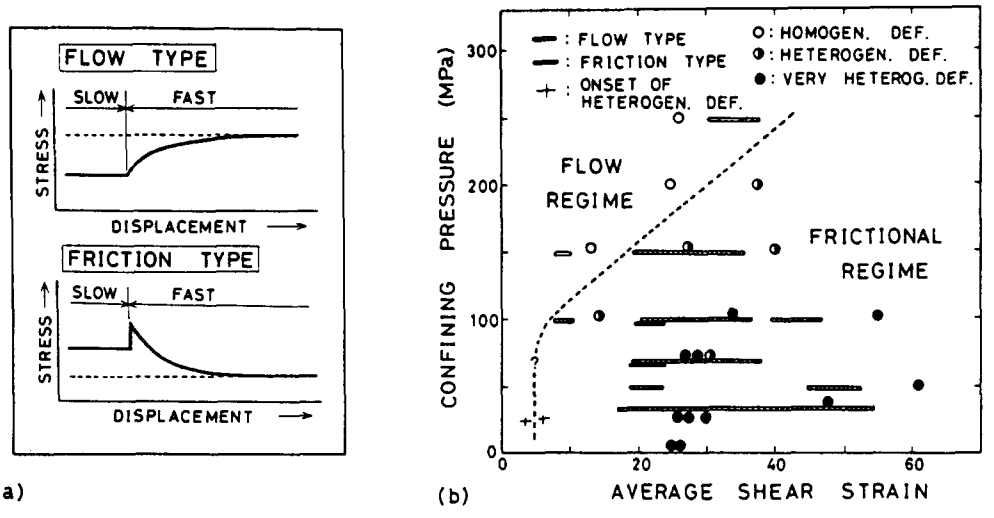


Fig. 10. Synthesis of mechanical and observational data (expanded from Shimamoto & Logan 1986, Hiraga & Shimamoto 1987). The behaviour of cooking salt shear zones during intermediate displacement rates (0.3–3 $\mu m\ s^{-1}$) is divided into flow-type and friction-type as schematically shown in (a) and is plotted with different symbols in the confining pressure vs shear strain space in (b). The mode of deformation within the cooking salt shear zone is classified into homogeneous, heterogeneous and very heterogeneous deformation and is plotted with different circular symbols in (b). The horizontal bars with short vertical bars indicate the onset of strain localization as determined from textural evidence (Hiraga & Shimamoto 1987). The dashed line in (b) roughly gives the critical shear strain for the onsets of strain localization and friction-type behaviour.

in the slip rate, and by a positive velocity dependence of the steady-state stress (or velocity strengthening). In contrast, friction-type behaviour is potentially unstable and exhibits an instantaneous viscous-like response followed by a gradual decay in the friction toward the steady-state value with a negative velocity dependence of the shear resistance (or velocity weakening; see Dieterich 1981). The experimental results, plotted in the confining-pressure vs shear-strain space in Fig. 10(b), indicate that the flow-type behaviour changes into friction-type with increasing shear strain and that the critical shear strain for this change in behaviour increases markedly with an increase in the confining pressure at pressures above about 100 MPa.

The mode of deformation within cooking salt shear zones was roughly classified into: (1) homogeneous deformation characterized by uniform and pervasive foliation (e.g. Fig. 5a); (2) heterogeneous deformation for which foliation is distorted slightly or considerably, but not to such a degree as to alter its original arrangement completely (e.g. Fig. 5e); and (3) very heterogeneous deformation with severely distorted and folded foliation (see Shimamoto & Logan 1986, Hiraga & Shimamoto 1987 for more details). The experimental results, plotted in Fig. 10(b), clearly indicate that homogeneous shearing deformation becomes heterogeneous when the shear strain reaches a critical value. Significantly, this shift in the mode of deformation nearly coincides with the shift in the mechanical behaviour from flow type to friction type. Thus, the potentially-unstable friction-type behaviour is a phenomenon that emerges as a result of strain localization.

Foliation in the cooking salt shear zones forms at confining pressures as low as 30 MPa. But after strain localization at this pressure, deformation is accommodated primarily by concentrated slip at the shear-zone boundary, although $R_1$ Riedel shears do form within the foliated shear zone (Hiraga & Shimamoto 1987). At confining pressures at and above 50 MPa, $R_1$, $Y$ and some $P$ Riedel shears are widespread throughout the foliated shear zones, and the pattern of foliation and the shears are similar to those of *S–C* mylonites. At confining pressures of 50–70 MPa, the Riedel shears are narrow, relatively planar and continuous, and stick–slip did occur (e.g. Fig. 2). At confining pressures above 100 MPa, the discontinuous zones of foliation becomes wider and less straight and the unstable fault motion disappears. At a confining pressure of 250 MPa where the halite shear zone is in the pressure-insensitive ductile regime, deformation was pervasive and nearly homogeneous and incipient heterogeneous deformation was recognized only very locally.

## DISCUSSIONS AND CONCLUSIONS

### *Petrogenesis of* S–C *mylonites*

The most important outcome from the halite experiments with regard to the petrogenesis of *S–C* mylonites is the recognition of strain-localization phenomenon after a critical shear strain, and the associated change in the mechanical behaviour in the semiductile regime (Fig. 10). If the Riedel shears developed in the halite shear zones (Fig. 7) can be taken as an experimental analog of the shear surfaces in *S–C* mylonites (Fig. 9), the shear surfaces of *S–C* mylonites should also develop as a result of such strain localization. Physical mechanisms responsible for this strain localization are as yet not perfectly clear. That the exponential flow law holds at test temperature (equation 1 and Fig. 4) indicates that halite is in the dislocation-glide regime and

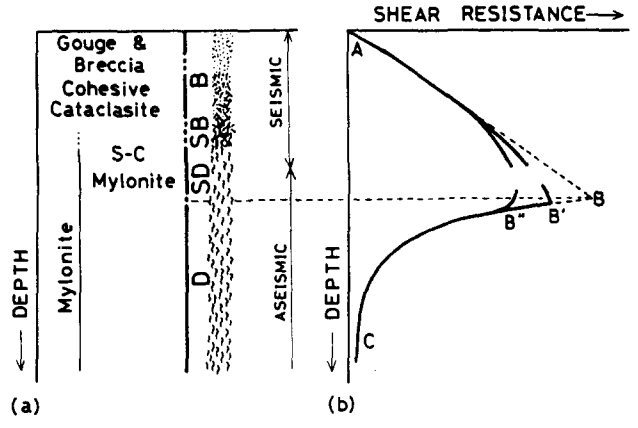


Fig. 11. (a) A new fault-zone model showing brittle (B), semibrittle (SB), semiductile (SD) and ductile (D) regimes together with their corresponding fault rocks. Most *S–C* mylonites are presumed to form in the semiductile regime, the upper half of which is seismogenic. (b) shows the presumed depth profile of fault strength.

therefore that the recovery processes are not fully operative at the test temperature. If this is really the case, uniform and pervasive plastic deformation cannot occur indefinitely because of strong interactions between dislocations, and deformation will eventually become localized with some kinds of brittle deformation overlapping with predominantly plastic deformation. Because of the complete recrystallization of sheared halite, it was impossible to confirm such a mechanism in our halite experiments. Observations of dislocation structures in *S–C* mylonites will provide additional insights into the mechanism of strain localization.

Strain localization of predominantly plastic deformation is a characteristic of the semiductile regime, in which deformation textures are very similar to those developed in the fully ductile regime and yet the shear resistance is pressure-dependent (Shimamoto & Logan 1986). Hence, this regime emerges as the primary candidate for the petrogenesis of *S–C* mylonites. Riedel shears in halite shear zones are relatively narrow and planar and unstable fault motion occurs in the low-pressure part of the semiductile regime. Thus, *S–C* mylonites with sharp internal shear surfaces may be associated with seismic slip events. If most *S–C* mylonites indeed form in the semiductile regime, close textural analyses of *S–C* mylonites may lead to the understanding of the deformation mechanisms along faults or plate boundaries at the depth range where large and great crustal earthquakes initiate and the shear resistance between neighbouring plates is near its maximum (Fig. 11). Hence, *S–C* mylonites may be of great tectonic and seismological significance.

It must be kept in mind, however, that the critical shear strain for strain localization is not attained in the fully ductile regime in the present experiment (see Fig. 10). Deformation might eventually have become localized if the halite shear zone were deformed further at a confining pressure of 250 MPa. Thus the fully ductile regime cannot be excluded from the possible candidates for the petrogenesis of *S–C* mylonites. Future experiments to even greater finite shear strains are clearly warranted.

*Recrystallization and grain-size refinement*

It is not entirely clear whether the almost complete recrystallization in the halite shear zone occurred under dynamic (syndeformational) or static (annealing or post-deformational) conditions. Knapp *et al.* (1987) called upon the former, but I am inclined to believe in the latter for the following reasons. Firstly, the exponential flow law holds at test temperature, and this law is characteristic of the low-temperature dislocation-glide regime, rather than of flow by dynamic recrystallization (e.g. Poirier 1985). Secondly, the relationship between grain size and stress, that has been confirmed in recrystallization flow, does not hold for the halite shear zones deformed at room temperature (Shimamoto & Logan 1986, Knapp *et al.* 1987). Thirdly, fine-grained neoblasts, described fully by Knapp *et al.* (1987), were also observed in some of our specimens just after the polishing of specimens for observations, but they soon totally disappeared to form an aggregate of coarse-grained recrystallized neoblasts, indicating that considerable recrystallization indeed took place after the shearing deformation. However, some degree of dynamic recrystallization cannot be denied and more work is needed to resolve this problem.

A common feature of mylonites from many parts of the world is increasing grain-size refinement with strain concentration (e.g. Tullis *et al.* 1982). Such a strain dependence, rather than a stress dependence, of recrystallized grains was recognized by Knapp *et al.* (1987) and is reconfirmed herein (Fig. 8). Previous interpretations for such strain dependence based on changes in deformation mechanism (e.g. Behrmann 1985, Behrmann & Mainprice 1987) are not applicable to the halite data, because the exponential flow law confirmed for halite shear zones at room temperature is consistent neither with high-temperature plasticity, nor with superplasticity. A simple explanation for the recrystallized halite grains is that the effect of strain is more pronounced on the nucleation rate than on the growth rate; i.e. a higher nucleation rate at a greater shear strain leads to finer recrystallized grains (e.g. Byrne 1965). Regardless of whether or not such a static growth model is applicable to natural mylonites, I feel that the effect of annealing recrystallization, even at relatively low temperature where recovery processes are not fully operative, has been overlooked in previous arguments. Clearly, this is an area of controversy to be discussed elsewhere. This paper has presented only preliminary data indicating a clear strain dependence of recrystallized grains that is consistent with the general trend of the grain-size refinement in natural mylonites.

*A new fault-zone model*

In view of the results from halite experiments, the fault-zone model in Fig. 1 needs to be modified along the following two lines. (1) The intermediate regimes (the semiductile regime in particular) between brittle and fully ductile regimes are much wider than indicated in

Fig. 1, and Byerlee's (1978) empirical equation for the frictional strength of brittle rocks cannot be extrapolated in a straight manner toward the fully ductile regime (Figs. 3 and 4 see also Kirby 1980). (2) Structures developed in the cooking salt shear zones in the semiductile regime are very close to the structures of *S–C* mylonites, so that the formation of mylonites is not restricted to the quasiplastic regime in Fig. 1 but could well be in the semiductile regime in which potentially unstable fault motion could occur.

A revised fault-zone model based mainly on the halite data (Shimamoto 1986b, 1988) consists of brittle, semibrittle, semiductile and ductile regimes with increasing depth (Fig. 11). Cataclasites and mylonites are presumed to form in the brittle regime and in the semiductile and ductile regimes, respectively. Rocks intermediate between cataclasites and mylonites should form in the semibrittle regime. There may not be fundamental differences between semibrittle and semiductile regimes in the sense that both cataclastic and plastic deformation may be involved more or less in these regimes. The term 'semiductile' is retained here to refer to the deformation in the intermediate regime whose textures are almost indistinguishable from those developed in the fully ductile regime through microstructural observations. Future work must clarify the distinguishing features between the deformation textures developed in the two regimes, which are readily applicable to natural mylonites.

The halite data (Fig. 3) suggest that the strength profile in the semiductile regime is such as that shown by curve AB′ in Fig. 11. However, the actual strength profile may be like curve AB″ because of the effect of temperature increase with increasing depth. Note that in the semiductile regime, the shear resistance depends on the slip rate in a complex manner (Figs. 3 and 4). This rate dependence suggests that the shear resistance also depends on temperature. The strength in the semiductile regime can no longer be assumed as independent of displacement rate or of temperature. The semiductile regime occupies more than half of the pressure-dependent domains in halite experiments (Fig. 3), but it is shown as narrower in Fig. 11 because increasing temperature with depth tends to reduce this domain. The exact strength profile cannot be drawn until the effect of temperature on the shearing behaviour under large shear strains is examined closely in the future.

Well-defined stick–slip occurred at a confining pressure of 70 MPa, well within the semiductile regime (Fig. 2; see also textures developed at the same pressure in Figs. 5b & c). Thus, the seismogenic depth is taken down to the upper part of the semiductile regime in Fig. 11. If such a model is correct, at least some mylonites should form at seismogenic depths. This is of interest, because close association of some pseudotachylytes with mylonites, in both space and time, has been reported recently (Sibson 1980, Grocott 1981, Passchier 1982, 1984, Hobbs *et al.* 1986). Pseudotachylite is about the only fault rock that unequivocally indicates the past occurrence of seismogenic movement along an exhumed fault (Sibson 1975, Wenk 1978, Weiss & Wenk 1983), and the present model is consistent with the association of pseudotachylytes and mylonites.

The close association of these rocks was taken previously as an evidence indicating that seismogenic depth occasionally extends well into the fully ductile regime (Sibson 1980, Hobbs *et al.* 1986). However, if mylonites form even in the semiductile regime, the association of pseudotachylytes and mylonites does not necessarily indicate that seismogenic motion extends into the ductile regime. Moreover, the lower part of a subducting plate boundary exhibits aseismic rebound following a great earthquake (Thatcher & Rundle 1979), and seismogenic depth apparently does not extend into the asthenosphere. It thus seems that the seismogenic depth at least for repeatable earthquakes along subducting plate boundaries does not extend into the fully ductile regime, consistent with the results from halite experiments.

Strehlau (1986) recently proposed a fault model that consists of an upper frictional and cataclastic zone, a middle transitional or semibrittle domain, and a lower plastic and mylonitic shear zone. The frictional and transitional regimes are taken as seismogenic, although he suggests that the rupture in a large earthquake may propagate down into the plastic regime. Strehlau's model is basically a two-component model in which Sibson's model in Fig. 1 is applied to each component, and his transitional regime corresponds to the depth range where one component is still brittle, while the other component is plastic. An implicit assumption in his model is that fault motion could be seismogenic if one component remains brittle. This, however, definitely is not the case, because fault-zone fabric evolves such that the weaker component accommodates much more strain and controls the fault motion more effectively than the stronger component (see Ross *et al.* 1987). The present fault model (Fig. 11) is essentially a single component model and does not fully account for the additional complexities arising from two- or multi-phase behaviours. The halite data have clearly shown that the property for each component cannot be handled as simply as treated by Strehlau (1986, fig. 4) and that the plastic regime is not the only place for the genesis of mylonites as assumed in his model. Thus, the present model should be considered as the starting point for dealing with more realistic, multi-phase behaviours.

More recently, Scholz (1988, fig. 4) proposed a revised fault model consisting of frictional, intermediate or semibrittle, and plastic regimes. Mylonites are assumed to form not only in the plastic regime, but also in the intermediate regime, and in this sense his model is consistent with the present model. Based mainly on the experimental data by Stesky (1978), Shimamoto (1986) and Shimamoto & Logan (1986), he idealizes that a change from velocity weakening (potentially unstable) to velocity strengthening (stable) in friction coincides with the onset of plasticity in the semibrittle regime. However, Scholz apparently misquotes the halite data which have revealed the velocity weakening behaviour well within the semiductile regime. Indeed, experiments at high temperatures (Friedman & Higgs 1981) revealed

that frictional behaviour changes from unstable to stable slip with the onset of plasticity. It should be kept in mind, however, that the nearly homogeneous plastic deformation with velocity strengthening in the semiductile regime changes into potentially unstable, heterogeneous deformation with velocity weakening only after the shear strain reaches a critical value (Fig. 10) (see also Shimamoto & Logan 1986, Hiraga & Shimamoto 1987). In particular, the fault displacement attained in the high-temperature experiments is small mainly because of technical reasons, and hence the critical strain for the strain localization or for the change in frictional behaviour might not have been reached during these experiments. Evidently, future experiments must address large-strain shearing behaviours of realistic rocks under high temperatures and pressures.

Both Strehlau (1986) and Scholz (1988) suggested downward propagation of rupture in a large earthquake and distinguished the nucleation depth for earthquakes from the depth extent of large ruptures. In particular, Scholz explained the interlaced occurrence of pseudotachylytes and mylonites (e.g. Sibson 1980, Hobbs *et al.* 1986) in terms of occasional downward propagation of earthquake rupture into otherwise aseismically deforming, intermediate regime. This may indeed be the case. However, stick–slip of halite shear zones in the semiductile regime is often accompanied by considerable aseismic slip, immediately before and after the dynamic fault motion (Shimamoto in press). Thus, at least some fraction of the plastic deformation overlapping with pseudotachylyte veins must have taken place during such aseismic portions of stick–slip cycles. At present, our knowledge of the mechanical properties within the intermediate regimes is limited to the general features of the relationship between steady-state shear resistance and the displacement rate (Fig. 4). If transient mechanical properties in these regimes are established in the future, complete and realistic modeling of earthquake cycles along faults or plate boundaries would be possible through theoretical analyses such as that by Tse & Rice (1986).

Finally, it should be pointed out that none of the existing fault models are fully incorporated with the effect of fluid-assisted diffusive mass transfer (i.e. deformation via pressure solution), even though abundant geological evidence indicates that the process is operative in geological deformation (e.g. Urai *et al.* 1987). The diffusion-accommodated fault slip is essentially a stable process (Rutter & Mainprice 1979), so that the process should not be fully operative at least at seismogenic depths. A subducting plate boundary shallower than 20–30 km in depth is a very rare place where $H_2O$ is supplied constantly, deformation via pressure solution is expected to be predominant, and earthquakes indeed do not occur (Shimamoto 1985). Complete evaluation of the effect of solution transfer on the deformation in the lithosphere is left for the future.

*Dedication and acknowledgements*—It is truly lamentable that Professor Kazuaki Nakamura of the University of Tokyo suddenly died of apoplexy on 12 August 1987. I sincerely dedicate this paper to the memory of his enthusiasm and wide scope to earth sciences, humour, stimulative atmosphere and above all hearty encouragements to young scientists.

Collaboration with H. Hiraga, J. M. Logan and M. Friedman on the halite shear zone experiments and very careful review of the manuscript by an anonymous reviewer are greatly acknowledged. I also thank H. Hiraga for allowing me to use his unpublished photomicrograph (Fig. 5e) for demonstrative purpose.

## REFERENCES

Bartlett, W. L., Friedman, M. & Logan, J. M. 1981. Experimental folding and faulting of rocks under confining pressure, Part. IX, Wrench faults in limestone layers. *Tectonophysics* **79**, 255–277.

Behrmann, J. H. 1985. Crystal plasticity and superplasticity in quartzite: a natural example. *Tectonophysics* **115**, 101–129.

Behrmann, J. H. & Mainprice, D. 1987. Deformation mechanisms in a high-temperature quartz-feldspar mylonite: evidence for superplastic flow in the lower continental crust. *Tectonophysics* **140**, 297–305.

Berthé, D., Choukroune, P. & Jégouzo, P. 1979. Orthogneiss, mylonite and non-coaxial deformation of granite: the example of the South Armorican Shear Zone. *J. Struct. Geol.* **1**, 31–42.

Bird, P. 1978. Initiation of intracontinental subduction in the Himalaya. *J. geophys. Res.* **83**, 4975–4987.

Blanpied, M. L., Tullis, T. E. & Weeks, J. D. 1987. Frictional behavior of granite at low and high sliding velocities. *Geophys. Res. Lett.* **14**, 554–557.

Brace, W. F. & Kohlstedt, D. L. 1980. Limits on lithospheric stress imposed by laboratory experiments. *J. geophys. Res.* **85**, 6248–6252.

Brunel, M. 1986. Ductile thrusting in the Himalayas: shear sense criteria and stretching lineations. *Tectonics* **5**, 247–265.

Byerlee, J. D. 1978. Friction of rocks. *Pure & Appl. Geophys.* **116**, 615–626.

Byrne, J. G. 1965. *Recovery, Recrystallization and Grain Growth.* Macmillan, London.

Carter, N. L. & Kirby, S. H. 1978. Transient creep and semibrittle behaviour of crystalline rocks. *Pure & Appl. Geophys.* **116**, 807–839.

Carter, N. L. & Hansen, F. D. 1983. Creep of rock salt. *Tectonophysics* **92**, 275–333.

Chen, W. P. & Molnar, P. 1983. Focal depths of intracontinental and intraplate earthquakes and their implications for the thermal and mechanical properties of the lithosphere. *J. geophys. Res.* **88**, 4183–4214.

Christie, J. M. & Ord, A. 1980. Flow stress from microstructures of mylonites: examples and current assessment. *J. geophys. Res.* **85**, 6253–6262.

Dieterich, J. H. 1978. Time-dependent friction and the mechanics of stick–slip. *Pure & Appl. Geophys.* **116**, 790–806.

Dieterich, J. H. 1979. Modeling of rock friction, 1, Experimental results and constitutive equations. *J. geophys. Res.* **84**, 2161–2168.

Dieterich, J. H. 1981. Constitutive properties of faults with simulated gouge. *Am. Geophys. Un. Geophys. Monogr.* **24**, 103–120.

Friedman, M. & Higgs, N. G. 1981. Calcite fabrics in experimental shear zones. *Am. Geophys. Un. Geophys. Monogr.* **24**, 11–27.

Goetze, C. & Evans, B. 1979. Stress and temperature in the bending lithosphere as constrained by experimental rock deformation. *Geophys. J. R. astr. Soc.* **59**, 463–478.

Grocott, J. 1981. Fracture geometry of pseudotachylyte generation zones: a study of shear fractures formed during seismic events. *J. Struct. Geol.* **3**, 169–178.

Grove, G. W. & Kelly, A. 1963. Independent slip systems in crystals. *Phil. Mag.* **8**, 877–887.

Handin, J. W., Friedman, M., Logan, J. M., Pattison, L. J. & Swolfs, H. S. 1972. Experimental folding of rocks under confining pressure: buckling of single-layer beams. *Am. Geophys. Un. Geophys. Monogr.* **16**, 1–28.

Handin, J. W., Russell, J. E. & Carter, N. L. 1986. Experimental deformation of rocksalt. *Am. Geophys. Un. Geophys. Monogr.* **36**, 117–160.

Hiraga, H. & Shimamoto, T. 1987. Textures of sheared halite and their implications for the seismogenic slip of deep faults. *Tectonophysics* **144**, 69–86.

Hobbs, B. E., Ord, A. & Teyssier, C. 1986. Earthquakes in the ductile regime? *Pure & Appl. Geophys.* **124**, 309–336.

Jégouzo, P. 1980. The South Armorican Shear Zone. *J. Struct. Geol.* **2**, 39–47.

Kirby, S. H. 1980. Tectonic stresses in the lithosphere: constraints provided by the experimental deformation of rocks. *J. geophys. Res.* **85**, 6353–6363.

Kirby, S. H. 1985. Rock mechanics observations pertinent to the rheology of the continental lithosphere and the localization of strain along shear zones. *Tectonophysics* **119**, 1–27.

Knapp, S. T., Friedman, M. & Logan, J. M. 1987. Slip and recrystallization of halite gouge in experimental shear zones. *Tectonophysics* **133**, 171–183.

Knipe, R. J. & White, S. H. 1979. Deformation in low grade shear zones in the Old Red Sandstone, S. W. Wales. *J. Struct. Geol.* **1**, 53–66.

Lister, G. S. & Snoke, A. W. 1984. *S–C* mylonites. *J. Struct. Geol.* **6**, 617–638.

Means, W. D. 1981. The concept of steady-state foliation. *Tectonophysics* **78**, 179–199.

Nicolas, A. & Poirier, J. P. 1976. *Crystalline Plasticity and Solid State Flow in Metamorphic Rocks.* John Wiley, New York.

O'Brien, D. K., Wenk, H.-R., Ratschbacher, L. & You, Z. 1987. Preferred orientation of phyllosilicates in phyllonites and ultramylonites. *J. Struct. Geol.* **9**, 719–730.

Passchier, C. W. 1982. Pseudotachylyte and the development of ultra-mylonite bands in the Saint-Barthelemy Massif, French Pyrenees. *J. Struct. Geol.* **4**, 69–79.

Passchier, C. W. 1984. The generation of ductile and brittle shear bands in a low-angle mylonite zone. *J. Struct. Geol.* **6**, 273–281.

Platt, J. P. 1984. Secondary cleavages in ductile shear zones. *J. Struct. Geol.* **6**, 439–442.

Platt, J. P. & Vissers, R. L. M. 1980. Extensional structures in anisotropic rocks. *J. Struct. Geol.* **2**, 397–410.

Poirier, J. P. 1985. *Creep of Crystals, High-Temperature Deformation Processes in Metals, Ceramics and Minerals.* Cambridge University Press.

Ponce de Leon, M. I. & Choukroune, P. 1980. Shear zones in the Iberian Arc. *J. Struct. Geol.* **2**, 63–68.

Rice, J. R. & Ruina, A. L. 1983. Stability of steady frictional sliding. *J. appl. Mech.* **50**, 343–349.

Ross, J. V., Bauer, S. J. & Hansen, F. 1987. Textural evolution of synthetic anhydrite-halite mylonites. *Tectonophysics* **140**, 307–326.

Ruina, A. L. 1983. Slip instability and state variable friction laws. *J. geophys. Res.* **88**, 10359–10370.

Rutter, E. H. 1986. On the nomenclature of mode of failure transitions in rocks. *Tectonophysics* **122**, 381–387.

Rutter, E. H. & Mainprice, D. H. 1979. On the possibility of slow fault slip controlled by a diffusive mass transfer process. *Gerlands Beitr. Geophys.* **88**, 154–162.

Scholz, C. H. 1988. The brittle–plastic transition and the depth of seismic faulting. *Geol. Rdsch.* **77**, 319–328.

Shimamoto, T. 1977. Effect of fault gouge on frictional properties of rocks: an experimental study. Unpublished Ph. D. dissertation, Texas A&M University.

Shimamoto, T. 1985. The origin of large or great thrust-type earthquakes along subducting plate boundaries. *Tectonophysics* **119**, 37–65.

Shimamoto, T. 1986a. Transition between frictional slip and ductile flow for halite shear zones at room temperature. *Science* **231**, 711–714.

Shimamoto, T. 1986b. Deformation mechanisms at the focal depths of large crustal earthquakes: an inference from geological data. *Seism. Soc. Japan, Annual Meet.* **2**, 236.*

Shimamoto, T. 1988. The origin of mylonites and a new fault model. *The Earth Monthly* **10**, 131–132.*

Shimamoto, T. In press. Mechanical behaviours of simulated halite shear zones: implications for the seismicity along subducting plate boundaries. In: *Rheology of Solids and of the Earth* (edited by Karato, S. & Toriumi, M.). Oxford University Press.

Shimamoto, T. & Logan, J. M. 1981. Effects of simulated fault gouge on the sliding behaviour of Tennessee sandstone: non-clay gouges. *J. geophys. Res.* **86**, 2902–2914.

Shimamoto, T. & Logan, J. M. 1986. Velocity-dependent behaviours of simulated halite shear zones: an analog for silicates. *Am. Geophys. Un. Geophys. Monogr.* **37**, 49–63.

Shimamoto, T., Handin, J. W. & Logan, J. M. 1980. Specimen-apparatus interaction during stick-slip in a triaxial compression machine: a decoupled two-degree-of-freedom model. *Tectonophysics* **67**, 175–205.

Shimazaki, K. 1974. Pre-seismic crustal deformation caused by an underthrusting oceanic plate in eastern Hokkaido, Japan. *Phys. Earth & Planet. Interiors* **8**, 148–157.

Sibson, R. H. 1975. Generation of pseudotachylyte by ancient seismic faulting. *Geophys. J. R. astr. Soc.* **43**, 775–794.

Sibson, R. H. 1977. Fault rocks and fault mechanisms. *J. geol. Soc. Lond.* **133**, 191–213.

Sibson, R. H. 1980. Transient discontinuities in ductile shear zones. *J. Struct. Geol.* **2**, 165–171.

Sibson, R. H. 1982. Fault zone models, heat flow, and the depth distribution of earthquakes in the continental crust of the United States. *Bull. seism. Soc. Am.* **72**, 151–163.

Sibson, R. H. 1983. Continental fault structure and the shallow earthquake source. *J. geol. Soc. Lond.* **140**, 741–767.

Simpson, C. & Schmid, S. M. 1983. An evaluation of criteria to deduce the sense of movement in sheared rocks. *Bull. geol. Soc. Am.* **94**, 1281–1288.

Smith, C. S. & Guttman, L. 1953. Measurement of internal boundaries in three-dimensional structure by random sectioning. *Trans. Am. Inst. Min. Metall. Petrol. Engrs* **197**, 81–87.

Strehlau, J. 1986. A discussion of the depth extent of rupture in large continental earthquakes. *Am. Geophys. Un. Geophys. Monogr.* **37**, 131–145.

Thatcher, W. & Rundle, J. B. 1979. A model for the earthquake-cycle in underthrust zones. *J. geophys. Res.* **84**, 5540–5556.

Tse, S. T. & Rice, J. R. 1986. Crustal earthquake instability in relation to the depth variation of frictional slip properties. *J. geophys. Res.* **91**, 9452–9472.

Tullis, J., Snoke, A. W. & Todd, V. R. 1982. Significance and petrogenesis of mylonitic rocks. *Geology* **10**, 227–230.

Urai, J. L., Spiers, C. J., Peach, C. J., Franssen, R. C. M. W. & Liezenberg, J. L. 1987. Deformation mechanisms operating in naturally deformed halite rocks as deduced from microstructural investigations. *Geologie Mijnb.* **66**, 165–176.

Vauchez, A. 1987. The development of discrete shear-zones in a granite: stress, strain and changes in deformation mechanisms. *Tectonophysics* **133**, 137–156.

Weiss, L. E. & Wenk, H.-R. 1983. Experimentally produced pseudotachylite-like veins in gabbro. *Tectonophysics* **96**, 299–310.

Wenk, H.-R. 1978. Are pseudotachylites products of fracture or fusion? *Geology* **6**, 507–511.

White, S. H., Burrows, S. E., Carreras, J., Shaw, N. D. & Humphreys, F. J. 1980. On mylonites in ductile shear zones. *J. Struct. Geol.* **2**, 175–187.

*In Japanese.